Instantaneous Amplitude of Equatorial Ionospheric Irregularities

Chun-Yen Huang[1], Jann-Yenq Liu[1, 2, 3]

[1] Graduate Institute of space science & engineering, National Central University, Taoyuan City, Taiwan

[2] Center for Space and Remote Sensing Research, National Central University, Taoyuan City, Taiwan

[3] Center for Astronautical Physics and Engineering, National Central University, Taoyuan City, Taiwan

Abstract

This study investigates the variations of equatorial ionospheric irregularity by means of ROCSAT-1, DEMETER, and FORMOSAT-5 during 1999-2004, 2006-2010, and 2018-2019, respectively. The occurrence probability and the instantaneous total amplitude derived from Hilbert-Huang transform are used to survey monthly, longitudinal variations in the equatorial/low-latitude ionospheric irregularities. The probability and the amplitude of ROCSAT-1 display that the region of the prominent occurrence rate varies month-by-month, which shifts from the South American sector in January to the African sector in July and returns to the South American sector by December. Meanwhile, low occurrence rate is more or less evenly distributed in other longitudes for the two equinox seasons. The probability of DEMETER is quite different from that of ROCSAT-1, especially during May-July in South American sector. On the other hand, the occurrence probability of FOMOSAT-5 is somewhat similar to that of ROCSAT-1 in South American－African sector, and however it is very different in other longitude regions. By contrast, the instantaneous total amplitude of the three satellites display nearly identical longitudinal variations in South American－African sector. In various longitudes and months, the probability and the amplitude of the three satellites within ±15° magnetic latitudes show the owl face feature.

Key word: Space weather, Ionosphere, Irregularity

1. Introduction

Plasma instability phenomena occurring in the equatorial F-region ionosphere is usually grouped under the generic name equatorial Spread-F (ESF), in which return echoes in ionograms display a spread in range. In the Range-time-intensity plot of incoherent scatter radar echoes, spectacular echoing features of so-called “radar plumes’’ are observed up to a thousand kilometers in altitude or more. For the radio wave communication between space and ground, the amplitude and phase scintillations will occur, while for the spacecraft in situ observation, plasma density becomes irregular. To investigate irregularities further, several rockets and satellites have penetrated the irregularity structures. Rino et al. (1981) studied the in-situ density profile probed by PLUMEX I rocket, and Tsunoda (1982) examined plasma density measurements observed by AE-E satellite. The two plots reveal that the radar plume is associated with a depleted structured region of plasma. Although radar can be used to analyze irregularities structure comprehensively, it is difficult to build a ground-based

technique anywhere. Recently, in-situ measurements and remote sensing by satellites are used to observe the global ionospheric irregularity structure. These developments provided opportunity to observe the ionosphere in remote and ocean areas. In the previous studies, satellite in situ observations are mainly used to examine the global and seasonal distributions of occurrence probability of irregularities (e.g., McClure et al., 1998; Su et al., 2006, 2008, 2010; Huang et al., 2014; Gentile et al., 2006; Kil et al., 2009). These statistical studies show that the occurrence probability of equatorial plasma bubbles depends on local time, latitude, longitude, season, geomagnetic activity, and solar activity, and that the irregularity growth at the African-Atlantic-American longitudes during the equinoctial season frequently. Recently, Liu et al. (2017) used the σ index, which proposes by Su et al. (2006) and showed that the high occurrence probability of low latitude irregularities probed by DEMETER/IAP develop constantly from 0 to 60°W near 2230 LT, especially May to August during 2006 to 2010. However, results of Liu et al. (2017) very differ from those probability of ROCSAT-1 that the location of high occurrence probability of irregularities has season variation at the African-Atlantic-American longitudes. The main difference between the two satellites is the inclination, 35° (a quasi-magnetic zonal direction) for ROCSAT-1 and 98.3° (a quasi-magnetic meridional direction) for DEMETER. Thus, to further understand the satellite inclination affected the observations, this thesis investigates the irregularity distribution by means of three satellites orbited in different inclination angles of 35° (ROCSAT-1/IPEI), 98.3° (DEMETER/ISL), and 98.3° (FORMOSAT5/AIP).

2. Experiment Design and Observations

ROCSAT-1 was in a near circular orbit at 600 km altitude with an inclination of 35° and at a velocity of about 7.5 km/s. DEMETER and FORMOSAT-5 operate in sun synchronous orbit at 680/720 km altitude with 98.3° inclination and 720 km altitude with 98.3° inclination, respectively. The in situ ion density data measured using an onboard Ionospheric Plasma and Electrodynamics Instrument (IPEI) of ROCSAT-1, Instrument Sonde de Langmuir (ISL) of DEMETER, and Advanced Ionospheric Probe (AIP) of FORMOSAT-5 are used in current study. For the cross comparison, we examine the ionospheric plasma irregularity using the σ index proposed by Su et al. (2006). Here, the σ index is given as,

$$\sigma = \frac{\left[\frac{1}{10}\sum_{i=1}^{10}(\log_{10} n_i - \log_{10} n_{oi})^2\right]^{\frac{1}{2}}}{\frac{1}{10}\sum_{i=1}^{10}\log_{10} n_{oi}}$$

where n_i is the ion density at each second, and n_{oi} is the linearly fitted value of 10-sec data. The $\sigma \geq 0.3\%$ to be used as a threshold to find ionospheric plasma irregularities from 1-sec ion density. On the other hand, the time deviate of the ion density, $\frac{dNi}{dt}$, is as a density fluctuation and compute the instantaneous total amplitude by using HHT. Since instantaneous amplitude and frequency (ω) are functions of time (t), the Hilbert amplitude spectrum (H) can be obtained. The instantaneous total amplitude (A) is defined as the integral of the instantaneous amplitude within a specific frequency interval

$$A(t) = \int_{\omega} H(\omega, t) d\omega$$

Because the density structures with wavelength longer than 200 km may result from the gravity wave seeding and electrodynamics uplift (Kelley, 2009), the instantaneous total amplitude is integrated within a period range from 0 to 26.67 sec (i.e. a wavelength range from 0 to 200 km) to show the intensity of density fluctuation. Figure 1 illustrates that the total amplitude agrees well with the σ index. Thus, the two indices, the σ and the HHT total amplitude, are used to observe the longitudinal variation of irregularities in this study.

3. Low-latitude F-region Irregularities

Figure 2 depicts that the occurrence probability and the total amplitude within $\pm 15°$ magnetic latitudes in various longitudes and months by ROCSAT-1,

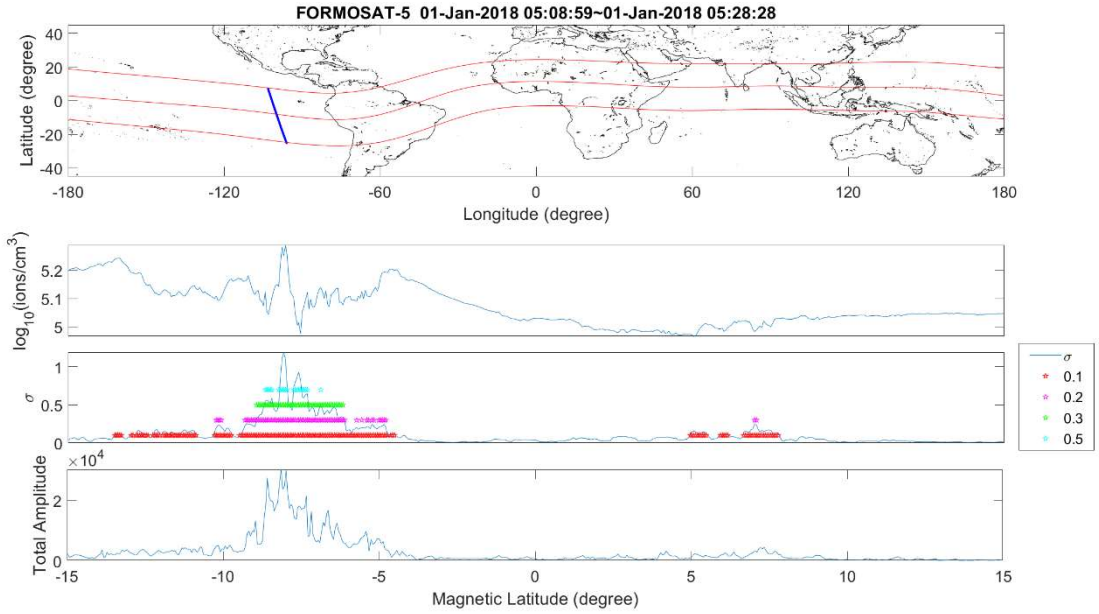

Figure 1. Example of equatorial ionospheric irregularities measured by the FORMOSAT-5 on 1 January 2018.

DEMETER, and FORMOSAT-5. Note that the color bar range in the amplitude of ROCSAT-1, 2.4-4.1 $\log_{10}$(ion/cm^3), DEMETER, 2.8-3.1 $\log_{10}$(ion/cm^3), and FORMOSAT-5, 2.3-3.1 $\log_{10}$(ion/cm^3) are quite different. The probability and the total amplitude of ROCSAT-1 show a nearly identical 'owl face' with eyes (two less dense irregularity eyes centering at 60°W and 90°E in July) and nose (between 60°W-60°E, South American – African sector) feature. The nose is mainly due to the monthly shifting and appear in the probability and the amplitude of three satellites. The west-longitude eye also clearly appears in the probability and the amplitude of DEMETER/FORMOSAT-5 but slightly shift westward and eastward, respectively. By contrast, the east-longitude eye simply appears in the amplitude observed by DEMETER. In addition, the third owl eye centering at 150°E in July has also been observed by DEMETER. It is surprising to see that DEMETER observes the most intense probability in 60°W-0° which looks like a 'tumor' in the east-longitude eye center during May to August. The probability and the amplitude are somewhat similar except the region between 90° and 150°E in September-March. For FORMOSAT-5, there is some difference between the probability and amplitude at the Atlantic sector around 30°W in June, and in October-December between 90°E and 180°E. The probability and the total amplitude of the three satellites are generally similar aside from the probability of DEMETER. Nevertheless, the owl eye feature can be observed by not only ROCSAT-1 but also DEMETER and FORMOSAT-5.

4. Discussion and Conclusion

The plots of Figure 2 illustrate the owl face with eyes and nose feature and show that the nose is mainly due to the monthly shifting. This owl face feature has been also observed by various observations. Gentil et al. (2006) used the depth of the deepest depletion in plasma density with respect to the nearby undisturbed one to classify irregularities and also discovered the clearly owl face feature by DMSP with the 99.8° inclination and around 800 km altitude during a whole solar activity period of 1989-2004. Huang et al. (2014) reported the owl face feature in S4 index and in amplitude of plasma density perturbations probe by FORMOSAT-3 during 2008-2012 and C/NOFS with 13° inclinations during 2008-2010. The owl face can also be clearly identified in weighted ROTI (rate of TEC index) during 2013 (Wu., 2020, Figure 3 personal communication). Kil et al. (2009) also revealed

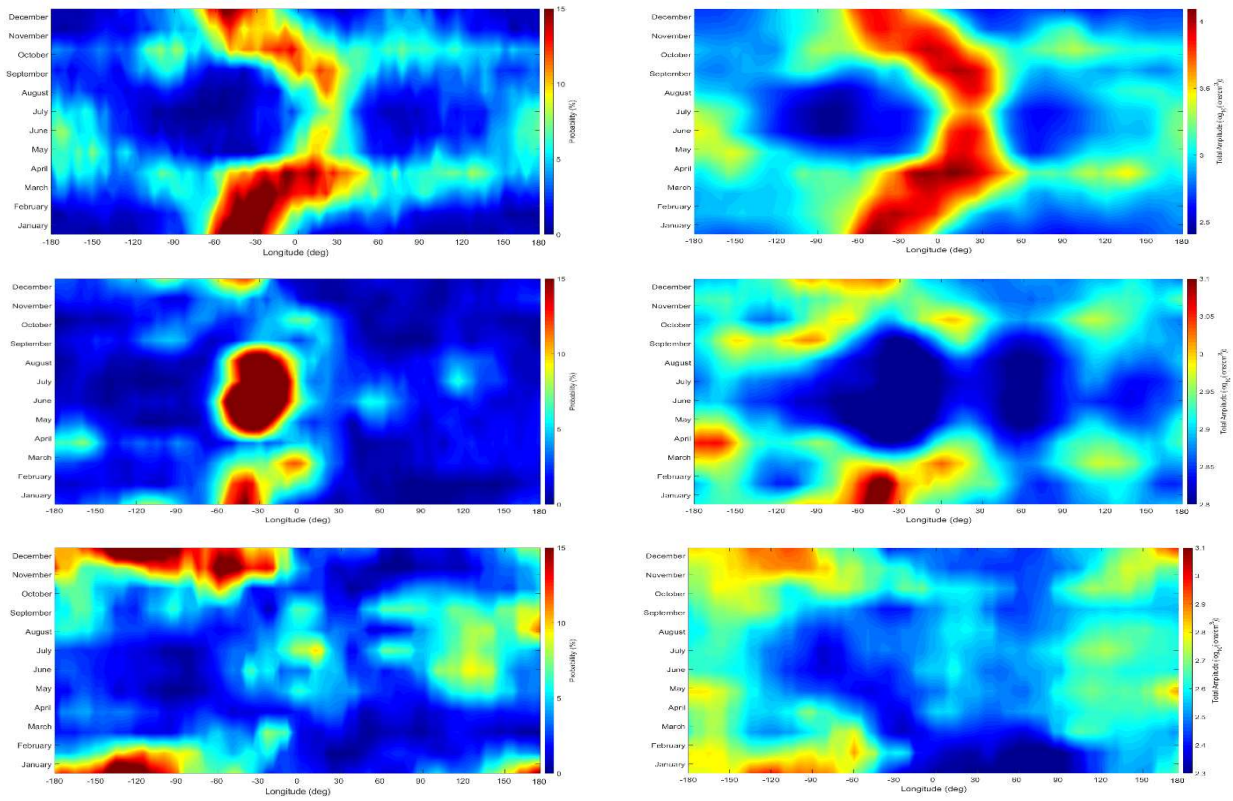

Figure 2. Monthly and Longitudinal variation. From top to bottom are the observations of ROCSAT-1, DEMETER, and FORMOSAT-5, respectively. Left column displays the occurrence probability and the right column represents the total amplitude.

that the owl face constantly exists every year during 1999-2004 observed by ROCSAT-1. These demonstrate the fact that the owl face feature is a real phenomenon which can be detected by in-situ measurement of high and low inclination satellites and regardless techniques and parameters. In Figure 2, It is surprising to see that for DEMETER, the tumor feature in May- August during the low activities is conversely greater than that during the high activities. To further study this discrepancy, the probability versus longitude has been examined year-by-year during 2005-2010. Figure 3 reveals that the east-longitude owl eye appears in 2005 and 2006, while the tumor feature starts appearing in 2007, reaches the most intense in 2009, and begins diminishing in 2010. Figures 4 shows that the denominator (i.e. background density normalization) varies more intense than numerator (i.e. the amplitude of ion density perturbation) of σ index at the tumor feature region during the solar minimum period.

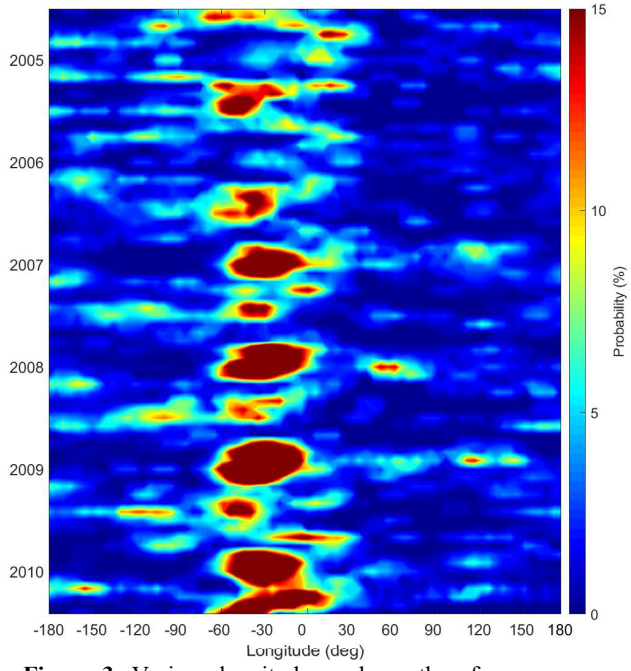

Figure 3. Various longitudes and months of occurrence probability by DEMETER during 2005-2010.

These agree with that the relative density perturbations (σ index) are small in the regions with high ambient density but become large in the regions with low ambient density (Huang et al., 2014). Liu et al. (2017) suggested that the σ

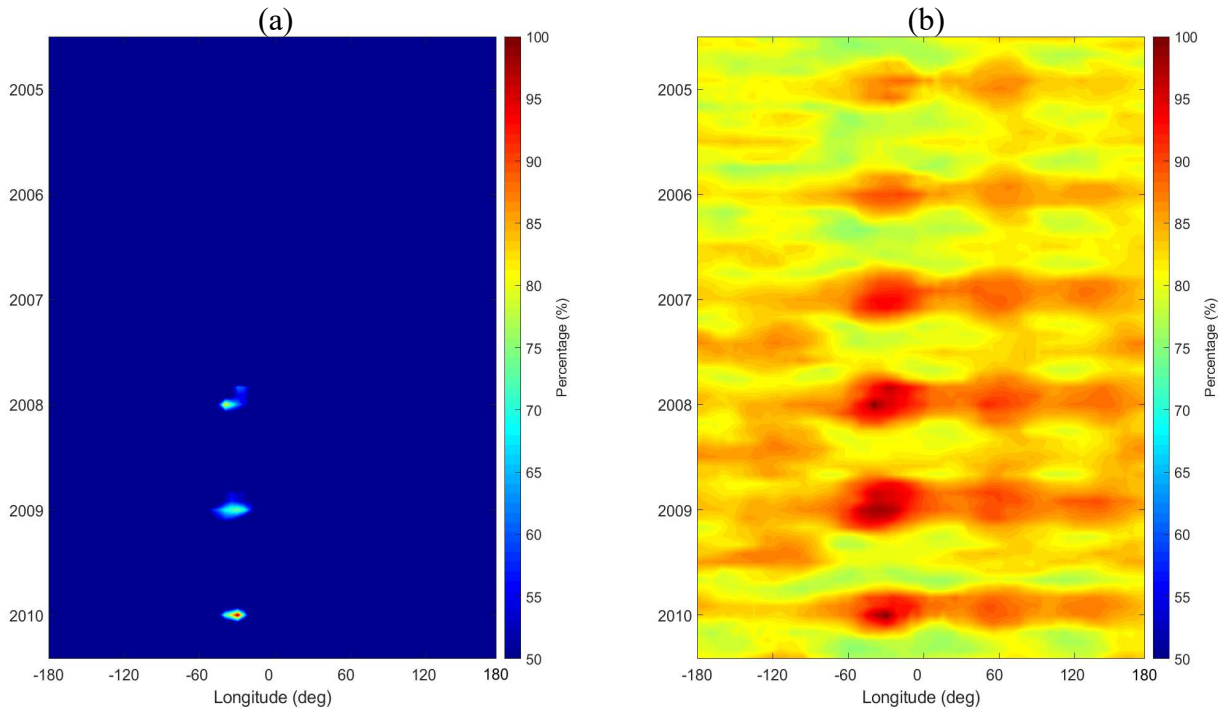

Figure 4. Various longitudes and months of (a) numerator and (b) denominator of σ inex by DEMETER from 2005 to 2010.

index might need to be redesigned for detecting low-latitude ionospheric plasma irregularities probed by sun-synchronous circular (high inclination) orbit satellites. As above, the pronounced probability appearing constantly from 0 to 60°W observed by DEMETER/IAP results from the extremely low ambient density. In conclusion, the occurrence probability and the total amplitude of the three satellites within $\pm 15°$ magnetic latitudes in various longitudes and months show the owl face feature. The discrepancy amounts the occurrence probability of DEMETER which results from the extremely low ambient ion density not the satellite inclination.

References

Gentile, L. C., W. J. Burke, and F. J. Rich (2006), A global climatology for equatorial plasma bubbles in the topside ionosphere, Ann. Geophys., 24, 163–172, doi:10.5194/angeo-24-163-2006.

Huang, C. S., O. de La Beaujardiere, P. A. Roddy, D. E. Hunton, J. Y. Liu, and S. P. Chen (2014), Occurrence probability and amplitude of equatorial ionospheric irregularities associated with plasma bubbles during low and moderate solar activities (2008–2012), J. Geophys. Res. Space Physics, 119, 1186–1199, doi:10.1002/2013JA019212.

Kelley MC (2009), The Earth's ionosphere: electrodynamics and plasma physics, 2nd edn. Elsevier, New York

Kil, H., L. J. Paxton, and S.-J. Oh (2009), Global bubble distribution seen from ROCSAT-1 and its association with the evening prereversal enhancement, J. Geophys. Res., 114, A06307, doi:10.1029/2008JA013672.

Liu, J. Y., Y. Y. Sun, C. K. Chao, S. P. Chen, and M. Parrot (2017), An observing system simulation experiment for FORMOSAT-5/AIP probing topside ionospheric plasma irregularities by using DEMETER/IAP. Terr. Atmos. Ocean. Sci., 28, 111-116, doi: 10.3319/TAO.2016.08.18.01(EOF5)

McClure, J. P., S. Singh, D. K. Bamgboye, F. S. Johnson, H. Kil (1998), Occurrence of equatorial F region irregularities: evidence for tropospheric seeding. J. Geophys. Res. 103 (A12), 29119–29135. http://dx.doi.org/10.1029/98JA02749.

Rino, C. L., R. T. Tsunoda R. T., J. Petriceks, R. C. Livingston, M. C. Kelley, and K. D. Baker, (1981). Simultaneous rocket-borne beacon and in situ measurements of equatorial spread

F— intermediate wavelength results. J. Geophys. Res. 86, 2411.

Su, S.Y., Liu, C.H., Ho, H.H., Chao, C.K., 2006. Distribution characteristics of topside ionospheric density irregularities: equatorial versus midlatitude regions. J. Geophys. Res. 111, A06305. http://dx.doi.org/10.1029/2005JA011330.

Su, S.Y., Chao, C.K., Liu, C.H., 2008. On monthly/seasonal/longitudinal variations of equatorial irregularity occurrences and their relationship with the postsunset vertical drift velocities. J. Geophys. Res. 113, A05307. http://dx.doi.org/10.1029/ 2007JA012809.

Su, S.Y., Chen, M.Q., Chao, C.K., Liu, C.H., 2010. Global, seasonal, and local time variations of ion density structure at the low-latitude ionosphere and their relationship to the postsunset equatorial irregularity occurrences. J. Geophys. Res. 115, A02309. http://dx.doi.org/10.1029/2009JA014339.

Tsunoda, R. T., R. C. Livingston, J. P. McClure, and W. B. Hanson (1982), Equatorial plasma bubbles: Vertically elongated wedges from the bottomside F layer. J. Geophys. Res. 87, 9171.